Journal of Power Sources 185 (2008) 754–758

Contents lists available at ScienceDirect

Journal of Power Sources

journal homepage: www.elsevier.com/locate/jpowsour

Short communication

$SmBaCo_2O_{5+x}$ double-perovskite structure cathode material for intermediate-temperature solid-oxide fuel cells

Qingjun Zhou, Tianmin He*, Yuan Ji

College of Physics, Jilin University, Changchun 130023, PR China

ARTICLE INFO

Article history:
Received 13 June 2008
Received in revised form 22 July 2008
Accepted 22 July 2008
Available online 31 July 2008

Keywords:
Solid-oxide fuel cell
Cathode
$SmBaCo_2O_{5+x}$
Double perovskite
Electrochemical performance

ABSTRACT

$SmBaCo_2O_{5+x}$ (SBCO), an oxide with double-perovskite structure, has been developed as a novel cathode material for intermediate-temperature solid-oxide fuel cells (IT-SOFCs). The electrical conductivity of an SBCO sample reaches 815–434 S cm^{-1} in the temperature range 500–800 °C. XRD results show that an SBCO cathode is chemically compatible with the intermediate-temperature electrolyte materials $Sm_{0.2}Ce_{0.8}O_{1.9}$ (SDC) and $La_{0.9}Sr_{0.1}Ga_{0.8}Mg_{0.2}O_{3-\delta}$ (LSGM). The polarization resistances of an SBCO cathode on SDC and LSGM electrolytes are 0.098 and 0.054 Ω cm^2 at 750 °C, respectively. The maximum power densities of a single cell with an SBCO cathode on SDC and LSGM electrolytes reach 641 and 777 mW cm^{-2} at 800 °C, respectively. The results of this study demonstrate that the double-perovskite structure oxide SBCO is a very promising cathode material for use in IT-SOFCs.

1. Introduction

Solid-oxide fuel cells (SOFCs) are advanced electrochemical reactors that convert chemical energy directly into electrical energy. Lowering their operating temperature to around 600–800 °C is one of the main goals in current SOFC research. A reduced operating temperature can reduce problems with sealing and thermal degradation, allow the use of low-cost metal interconnection materials, and suppress reactions between the cell components, thus lowering the cost of SOFCs. However, the electrochemical activity of the cathode dramatically decreases with decreasing temperature. The cathode becomes the limiting factor in determining the overall cell performance. Therefore, the development of new electrodes with high-electrocatalytic activity for the oxygen-reduction reaction is critical for intermediate-temperature solid-oxide fuel (IT-SOFCs) [1,2]. Much effort has been devoted to the development of perovskite-type cathode materials, for example, doped $LnCoO_3$, $SrCoO_3$ and $LnFeO_3$ (Ln represents a lanthanide element), for IT-SOFCs [3–8]. This is due to their unique ability to conduct both oxygen ions and electronic charge carriers, as well as to their high-electrocatalytic activity for the oxygen-reduction reaction even at reduced temperatures. Since the discovery of giant magnetoresistance in the oxygen-deficient double-perovskite structure ($LnBaCo_2O_{5+x}$, Ln = rare earth, $0 \le x \le 1$) [9], these materials have been attracting much more attention in many research fields [10–18]. Recent studies on double-perovskite structure cobaltites, such as $PrBaCo_2O_{5+x}$ (PBCO) [19,20] and $GdBaCo_2O_{5+x}$ (GBCO) [21,22], have found that they have unusually rapid oxygen-transport kinetics at low temperatures (300–500 °C). For example, the oxygen bulk diffusion coefficient and the surface-exchange coefficient of PBCO are $\sim 10^{-5}$ and $\sim 10^{-3}$ cm s^{-1} [20], and the values for GBCO are 3×10^{-7} and 2×10^{-6} cm s^{-1} in an oxygen flow at 350 °C, respectively [21]. The rapid surface-exchange kinetics of these materials give rise to their high-catalytic activity [22]. In view of the rapid oxygen-ion diffusion and surface-exchange kinetics in the double-perovskite structure oxides PBCO and GBCO, preliminary results on the electrical and thermal-expansion behaviors of the mixed ionic–electronic conducting oxides $LnBaCo_2O_{5+x}$ have recently been reported [23–28]. These oxides have potential applications as cathodes in IT-SOFCs. Cobalt-based cathodes generally exhibit high oxygen-ion conductivity. However, these materials have high thermal-expansion coefficients (TECs) that are not compatible with those of intermediate-temperature electrolytes. Kim and Manthiram [27] reported that the electrical conductivity of $LnBaCo_2O_{5+x}$ (Ln = Nd, Sm, Gd, and Y) oxides decreases with a decrease of the Ln^{3+} ion radii, leading to the decreasing power density of a single cell with an $LnBaCo_2O_{5+x}$ cathode and high TECs. Therefore, $LnBaCo_2O_{5+x}$ cathodes with an intermediate lanthanide-ion radius, such as Sm^{3+}, may provide a compromise between the values of the catalytic activity and TEC [27]. In this paper, the double-perovskite structure oxide $SmBaCo_2O_{5+x}$ (SBCO) was prepared and characterized. The suitabil-

* Corresponding author. Fax: +86 431 88498000.
E-mail address: hly@mail.jlu.edu.cn (T. He).

0378-7753/$ – see front matter © 2008 Elsevier B.V. All rights reserved.
doi:10.1016/j.jpowsour.2008.07.064

ity of SBCO as a cathode material based on $Sm_{0.2}Ce_{0.8}O_{1.9}$ (SDC) and $La_{0.9}Sr_{0.1}Ga_{0.8}Mg_{0.2}O_{3-\delta}$ (LSGM) electrolytes was analyzed over the IT-SOFC temperature range. The electrochemical performance of an SBCO cathode on SDC and LSGM electrolytes was also investigated.

2. Experimental

2.1. Sample preparation

Samples of SBCO were prepared with a conventional solid-state reaction as reported elsewhere [29]. Briefly, Sm_2O_3, $BaCO_3$ and Co_2O_3 were weighed in the stoichiometric proportions of SBCO, then mixed, ground and pelletized. The mixture was ground thoroughly using an agate pestle and mortar for 1 h, then pressed into a disk and fired repeatedly at 1000, 1050, and 1150 °C for 12 h in air, respectively. SDC and LSGM were used as electrolyte materials in this study. SDC, LSGM and NiO powders were synthesized using the glycine–nitrate combustion method [30].

2.2. Characterization

Electrical conductivity of an SBCO sample was measured in air by the van der Pauw method using a standard DC voltage/current generator (Yokogawa Electric, 2553) and a precision digital multimeter (Yokogawa Electric, 2501A). In this measurement, Ag paste was used for the electrodes.

The phase composition of the synthesized powders was characterized using an X-ray diffractometer (XRD) (Rigaku-D-Max γA) with an angle step of 0.02° and a scanning range of 20–80°, at room temperature. For studies of the chemical compatibility of SBCO with SDC and LSGM electrolytes, the synthesized SBCO powders were first mixed with SDC and LSGM (in a weight ratio of 1:1) to form a powder mixture, followed by sintering to 1000 °C for 5 h. XRD investigations were then performed to reveal any phase-composition change after the heat treatment.

Symmetrical electrochemical cells for the impedance studies were prepared by screen printing an SBCO ink sample onto both sides of the SDC and LSGM electrolytes. After drying, the samples were sintered at 950 °C for 2 h. Impedance measurements were performed in the temperature range 650–800 °C for the SDC and LSGM electrolytes with 50 °C increments for all the samples. AC impedance spectrometry was carried out using an electrochemical analyzer (CHI604C) under open-circuit conditions in the frequency range 0.1–10^5 Hz. The amplitude of the AC signal imposed on the samples was 10 mV.

Electrolyte-supported fuel cells were fabricated using a screen printing method. SDC and LSGM were used as the electrolytes with a fixed thickness of 300 μm each. The anode was formed from a mixture of NiO and SDC powders in a weight ratio of 65:35 (for the cell with LSGM electrolyte, an SDC interlayer was applied between the electrolyte and the anode and sintered at 1300 °C for 1 h). The anode and cathode were then fired at 1250 °C for 4 h and 950 °C for 2 h under stagnant air, respectively. Silver was attached to the electrode surfaces using silver paste as the current collector. The performance of the cell was tested under dry H_2 and static air over the temperature range 600–800 °C. A scanning electron microscope (SEM) (JEOL JSM-6480LV) was used to inspect the microstructure of the SBCO/SDC and SBCO/LSGM interfaces after testing.

3. Results and discussion

3.1. Electrical conductivity

Fig. 1 shows the variation of the electrical conductivity with temperature for the SBCO samples. The total electrical conductivity was measured on an SBCO disk sintered at 1150 °C for 12 h in air. The SBCO sample exhibits an insulator–metal transition at around 37 °C, which is consistent with a previous report [29]. This transition is related to the oxygen stoichiometry [29]. Thereafter, the electrical conductivity of SBCO gradually increases with increasing temperature and reaches a maximum of 1029 S cm^{-1} at around 200 °C. It then decreases with a further increase in temperature of the SBCO sample, which presented metallic-like behavior. The faster decrease in conductivity at higher temperatures could be due to the formation of a significant amount of oxide-ion vacancies. The formation of oxide-ion vacancies is accompanied by a reduction of Co^{4+} to Co^{3+}, resulting in a decrease in the charge-carrier concentration and Co–O covalency. The oxide-ion vacancies can also perturb the O–Co–O periodic potential and covalent interaction [31]. All these factors lead to a decrease in electrical conductivity of the SBCO sample at increased temperatures. The electrical conductivity reaches 815–434 S cm^{-1} in the temperature range 500–800 °C, which is still sufficient for use as an SOFC cathode.

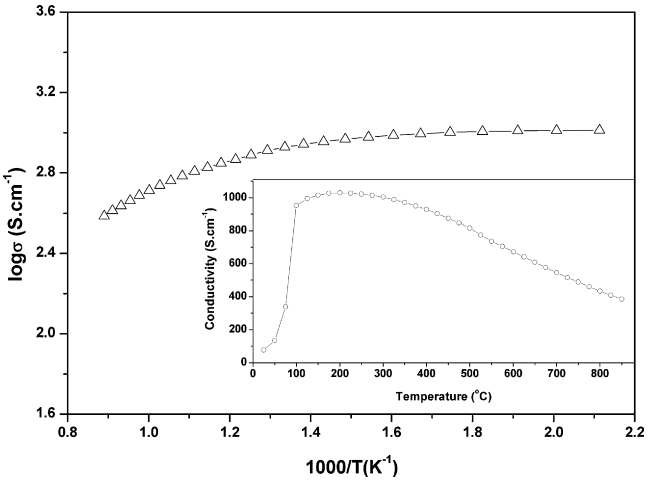

Fig. 1. Temperature dependence of the conductivity for SBCO samples.

3.2. Chemical compatibility and microstructure

Figs. 2 and 3 show XRD patterns of SBCO, SDC and LSGM powders and SBCO–SDC and SBCO–LSGM mixtures sintered at 1000 °C

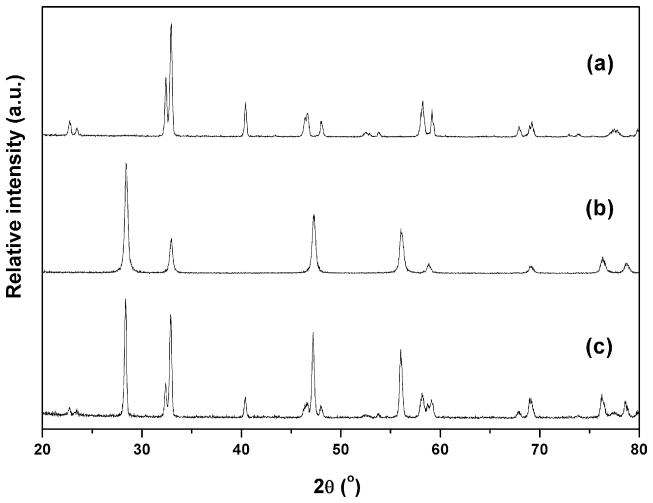

Fig. 2. XRD patterns of (a) SBCO powders, (b) SDC powders and (c) SBCO–SDC mixture sintered at 1000 °C for 5 h.

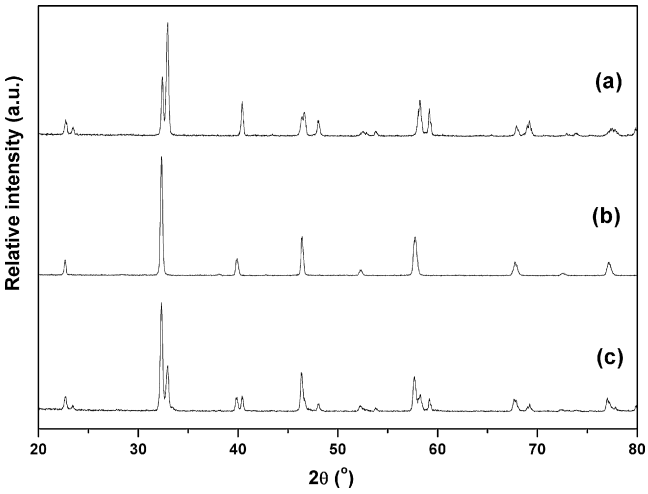

Fig. 3. XRD patterns of (a) SBCO powders, (b) LSGM powders and (c) SBCO–LSGM mixture sintered at 1000 °C for 5 h.

for 5 h. The patterns are identical to that of SBCO obtained after sintering at 1100 °C for 24 h [29], indicating the formation of a single-phase perovskite of the SBCO powder (Figs. 2(a) and 3(a)). The XRD patterns in Figs. 2(c) and 3(c) show that an SBCO cathode is chemically compatible with SDC and LSGM electrolytes. No chemical reaction of the binary-mixed SBCO–SDC and SBCO–LSGM systems is detected upon sintering at 1000 °C for 5 h. This indicates that SBCO has a good chemical compatibility with SDC and LSGM electrolytes, supporting its use as a cathode in SOFCs.

Fig. 4 shows SEM micrographs of the SBCO/SDC and SBCO/LSGM interfaces after cell testing. The micrographs clearly indicate that there is a good contact between the electrode and the electrolyte, which is in good agreement with the cell performance (see Sections 3.3 and 3.4). Some visible closed pores are also observed in the SDC and LSGM electrolytes. The contact between SBCO and LSGM is better than that between SBCO and SDC. However, the SEM micrographs also clearly show that the porosity in the cathode is low and that the particle-size distribution is not uniform. Further improvement in the distribution of SBCO particle sizes and porosity in the cathode would enhance the cell performance.

3.3. Impedance spectra

Figs. 5 and 6 show the impedance spectra of SBCO cathodes on SDC and LSGM electrolytes measured at different temperatures in air. The impedance was measured using a symmetrical cell arrangement, as discussed by other workers [2,32]. For all the samples measured in this investigation, the impedance response for oxygen reduction on the SBCO cathode is characterized by both a high-frequency arc and a low-frequency arc. The intercept with the real axis at high frequency represents the resistance of the electrolyte and lead wires, whereas the resistance between the two intercepts with the real axis corresponds to the area-specific resistance (ASR, or polarization resistance) of the two interfaces [33]. As expected, an increase of the measurement temperature resulted in a significant reduction of the ASR. The evolution of the ASR with temperature is given in Table 1. The ASRs of an SBCO cathode on SDC and LSGM electrolytes are 0.098 and 0.054 Ω cm^2 at 750 °C, respectively. The ASR represents the overall cathodic properties related to oxygen reduction, oxygen surface/bulk diffusion and gas-phase oxygen diffusion [34]. These values are much lower than that expected for the ASR of the cathode, which is lower than 0.15 Ω cm^2 at operating temperature [35]. Moreover, the ASR of SBCO is lower than that of $La_{0.6}Sr_{0.4}Co_{0.2}Fe_{0.8}O_3$ (LSCF), $Sm_{0.5}Sr_{0.5}CoO_3$ and $Gd_{0.8}Sr_{0.2}CoO_3$ cathodes [36–38]. This indicates that an SCBO cathode has high-electrocatalytic activity for oxygen-reduction reactions at intermediate temperatures. The

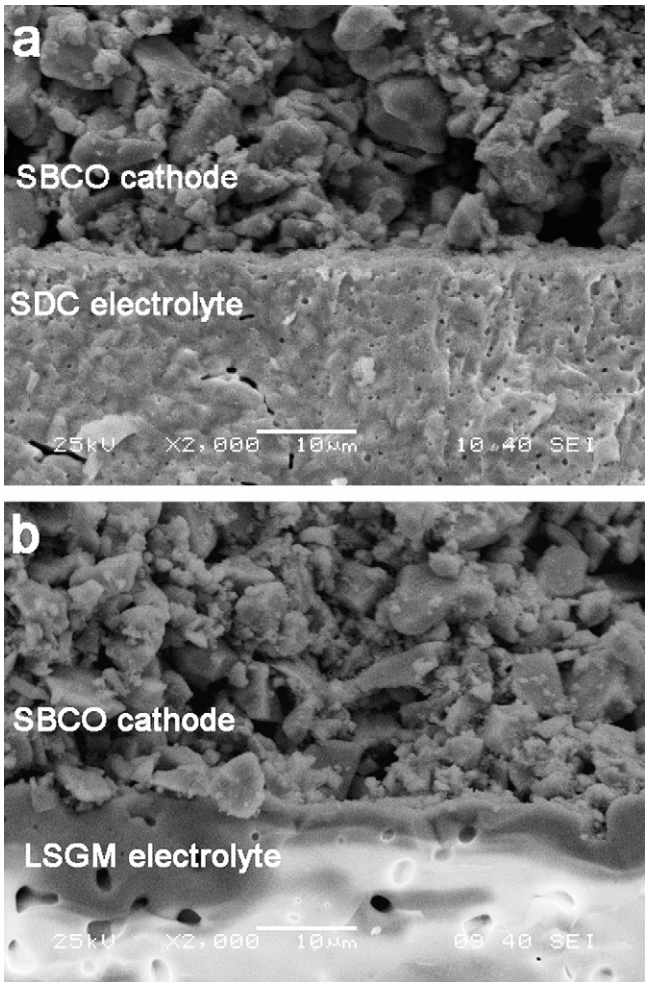

Fig. 4. SEM micrographs of (a) SBCO/SDC and (b) SBCO/LSGM interfaces; the SBCO cathodes were sintered at 950 °C for 2 h.

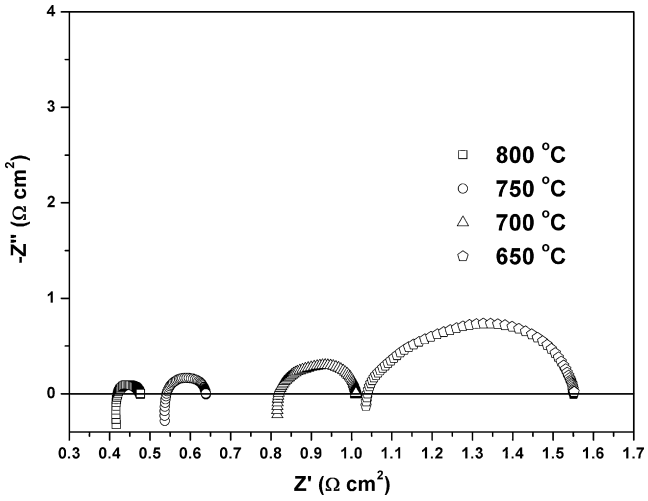

Fig. 5. Impedance spectra of SBCO cathode with SDC electrolyte measured at 650–800 °C.

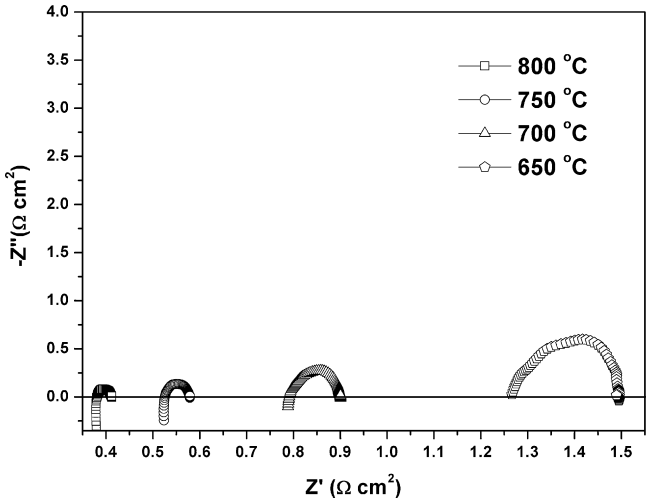

Fig. 6. Impedance spectra of SBCO cathode with LSGM electrolyte measured at 650–800 °C.

Table 1
ASR data for SBCO cathodes on SDC and LSGM electrolytes (with cathode thickness of ~25 μm)

Temperature (°C)	ASR on SDC (Ω cm^2)	ASR on LSGM (Ω cm^2)
650	0.51	0.23
700	0.19	0.11
750	0.098	0.054
800	0.056	0.031

excellent cathode performance of SBCO is due to the fact that it is a mixed conducting oxide (MIEC), which provides multiple pathways for the oxygen ions to migrate to the electrode/electrolyte interface. However, the decrease of the measurement temperature resulted in a significant increase of the ASR. Therefore, further investigations using a composite cathode are needed in order to determine the effect of cathode microstructure on the electrochemical performance. Fig. 7 shows the Arrhenius plots of the reciprocal of the polarization resistance of an SBCO cathode on SDC and LSGM electrolytes sintered at 950 °C. The activation energy can be calculated from the slope of the fitted line. The activation energies were calculated to be 120.8 and 111.1 kJ mol^{-1} for an SBCO cathode on SDC and LSGM electrolytes, respectively. This result is close to that for

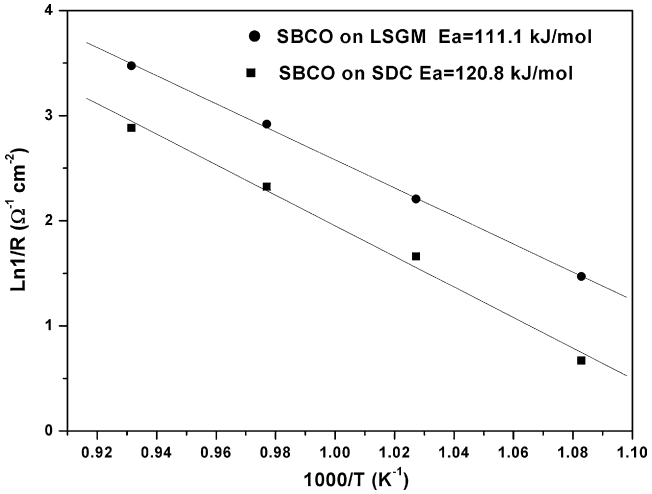

Fig. 7. Arrhenius plots of reciprocal of the polarization resistance of SBCO cathodes on SDC and LSGM electrolytes sintered at 950 °C for 2 h.

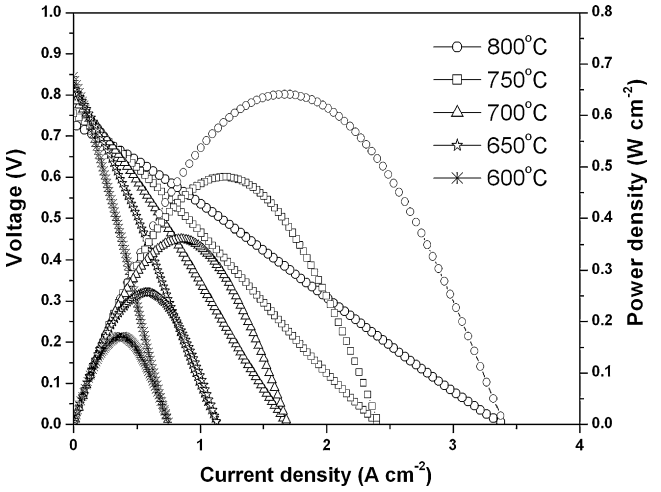

Fig. 8. Power density and voltage as a function of current density for an Ni–SDC/SDC/SBCO cell using H_2 as fuel and air as oxidant in the temperature range 600–800 °C.

a $Ba_{0.5}Sr_{0.5}Co_{0.8}Fe_{0.2}O_{3-\delta}$ cathode reported by Shao and Haile [2]. However, it is lower than that for an LSCF cathode [36].

3.4. Single-cell performance

Figs. 8 and 9 show the power density and voltage as a function of current density for Ni–SDC/SDC/SBCO and Ni–SDC/SDC/LSGM/SBCO cells using H_2 as the fuel and static air as the oxidant in the temperature range 600–800 °C, respectively. The power densities reach 641 mW cm^{-2} at 800 °C and 170 mW cm^{-2} at 600 °C for the SDC electrolyte cell. For the LSGM electrolyte cell, the power densities are 777 mW cm^{-2} at 800 °C and 95 mW cm^{-2} at 600 °C. High-power densities demonstrate that SBCO is one of the better promising cathode materials for SOFCs operating below 800 °C. These results also demonstrate that rapid oxygen-ion diffusion and surface-exchange kinetics may play dominant roles in the cell performance [19–21,23]. The power density of a cell with LSGM electrolyte is higher than that of SDC electrolyte. This is mainly because the contact between SBCO and LSGM is superior to that of SBCO and SDC, as shown in the SEM micrographs. It is noted that the drastic drop of the power

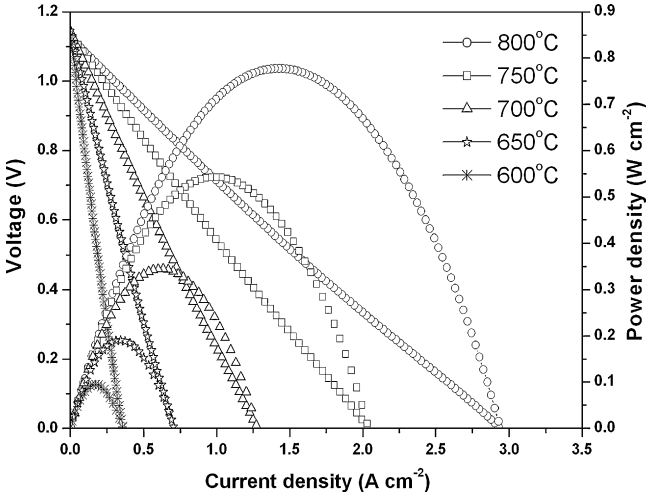

Fig. 9. Power density and voltage as a function of current density for an Ni–SDC/SDC/LSGM/SBCO cell using H_2 as fuel and air as oxidant in the temperature range 600–800 °C.

density at 600 °C is due to the ohmic losses of the electrolyte and the high polarization of the electrodes. Therefore, more efforts are necessary to increase the electrochemical performance below this temperature, e.g., optimizing the microstructure of the electrodes by improving the uneven grain size, low porosity and poorly necked particles. Further investigations introducing composite cathodes or improving the material preparation method are needed.

4. Conclusions

$SmBaCo_2O_{5+x}$ cathode material with double-perovskite structure was synthesized with a solid-state reaction. The SBCO cathode material was found to exhibit a relatively good performance below 800 °C on SDC and LSGM electrolytes. The conductivity of the SBCO cathode was 815–434 S cm^{-1} in the temperature range 500–800 °C. The SBCO cathode material also revealed a good chemical compatibility with the SDC and LSGM electrolytes. The polarization resistances for the SBCO cathode on SDC and LSGM electrolytes were 0.098 and 0.054 Ω cm^2 at 750 °C, respectively. The maximum output power density of a single cell with an SBCO cathode and SDC and LSGM electrolytes attained 641 and 777 mW cm^{-2} at 800 °C, respectively. Although the long-term stability of cells with SBCO cathodes has yet to be evaluated, the obtained power outputs are encouraging and indicate that SBCO oxide is a very promising cathode material for application in IT-SOFCs.

Acknowledgement

This work was supported by the Natural Science Foundation of China under contract No. 10604020.

References

[1] N.P. Brandon, S. Skinner, B.C.H. Steele, Annu. Rev. Mater. Res. 33 (2003) 183–213.
[2] Z. Shao, S.M. Haile, Nature 431 (2004) 170–173.
[3] S.B. Adler, Solid State Ionics 111 (1998) 125–134.
[4] C.R. Xia, W. Rauch, F.L. Chen, M.L. Liu, Solid State Ionics 149 (2002) 11–19.
[5] C. Rossignol, J.M. Ralph, J.-M. Bae, J.T. Vaughey, Solid State Ionics 175 (2004) 59–61.
[6] F. Riza, C. Ftikos, F. Tietz, W. Fischer, J. Eur. Ceram. Soc. 21 (2001) 1769–1773.
[7] L. Qiu, T. Ichikawa, A. Hirano, N. Zmanishi, Y. Takeda, Solid State Ionics 158 (2003) 55–65.
[8] H.Y. Tu, Y. Takeda, N. Imanishi, O. Yamamoto, Solid State Ionics 117 (1999) 277–281.
[9] C. Martin, A. Maignan, D. Pelloquin, N. Nguyen, B. Raveau, Appl. Phys. Lett. 71 (1997) 1421–1423.
[10] F. Fauth, E. Suard, V. Caignaert, B. Domengès, I. Mirebeau, L. Keller, Eur. Phys. J. B 21 (2001) 163–174.
[11] F. Fauth, E. Suard, V. Caignaert, I. Mirebeau, Phys. Rev. B 66 (2002), 184421-1-5.
[12] P.S. Anderson, C.A. Kirk, J. Knudsen, I.M. Reaney, A.R. West, Solid State Sci. 7 (2005) 1149–1156.
[13] S. Roy, I.S. Dubenko, M. Khan, E.M. Condon, J. Craig, N. Ali, Phys. Rev. B 71 (2005), 024419-1-9.
[14] M. Pękała, J. Mucha, M. Baran, I. Troyanchuk, B. Krzymańska, H. Szymczak, J. Magn. Magn. Mater. 292 (2005) 385–393.
[15] Z. Yuan, J. Liu, C.L. Chen, Appl. Phys. Lett. 90 (2007), 212111-1-3.
[16] A. Podlesnyak, S. Streule, K. Conder, E. Pomjakushina, J. Mesot, A. Mirmelstein, P. Schützendorf, R. Lengsdorf, M.M. Abd-Elmeguid, Physica B 378–380 (2006) 537–538.
[17] S.N. Barilo, S.V. Shiryaev, G.L. Bychkov, A.S. Shestak, W.R. Flavell, A.G. Thomas, H.M. Rafique, Y.P. Chernenkov, V.P. Plakhty, E. Pomjakushina, K. Conder, P. Allenspach, J. Cryst. Growth 310 (2008) 1867–1874.
[18] C. Frontera, J.L. García-Muñoz, A.E. Carrillo, A. Caneiro, J. Magn. Magn. Mater. 316 (2007) 731–733.
[19] G. Kim, S. Wang, A.J. Jacobson, Appl. Phys. Lett. 88 (2006), 024103-1-3.
[20] G. Kim, S. Wang, A.J. Jacobson, L. Reimus, P. Brodersen, C.A. Mims, J. Mater. Chem. 17 (2007) 2500–2505.
[21] A.A. Taskin, A.N. Lavrov, Y. Ando, Appl. Phys. Lett. 86 (2005), 091910-1-3.
[22] S.B. Adler, J.A. Lane, B.C.H. Steele, J. Electrochem. Soc. 143 (1996) 3554–3564.
[23] A. Tarancón, S.J. Skinner, R.J. Chater, F. Hernández-Ramírez, J.A. Kilner, J. Mater. Chem. 17 (2007) 3175–3181.
[24] A.M. Chang, S.J. Skinner, A. Kilner, Solid State Ionics 177 (2006) 2009–2011.
[25] N. Li, Z. Lü, B. Wei, X.Q. Huang, K.F. Chen, Y.H. Zhang, W.H. Su, J. Alloys Compd. 454 (2008) 274–279.
[26] A. Tarancón, A. Morata, G. Dezanneau, S.J. Skinner, J.A. Kilner, S. Estradé, F. Hernández-Ramírez, F. Peiró, J.R. Morante, J. Power Sources 174 (2007) 255–263.
[27] J.-H. Kim, A. Manthiram, J. Electrochem. Soc. 155 (4) (2008) B385–390.
[28] B. Lin, S.Q. Zhang, L.C. Zhang, L. Bi, H.P. Ding, X.Q. Liu, J.F. Gao, G.Y. Meng, J. Power Sources 177 (2008) 330–333.
[29] A. Maignan, C. Martin, D. Pelloquin, N. Nguyen, B. Raveau, J. Solid State Chem. 142 (1999) 247–260.
[30] L.G. Cong, T.M. He, Y. Ji, P.F. Guan, Y.L. Huang, W.H. Su, J. Alloys Compd. 348 (2003) 325–331.
[31] H. Takahashi, F. Munakata, M. Yamanaka, Phys. Rev. B 57 (1998) 15211–15218.
[32] J.R. Macdonald, Impedance Spectroscopy: Emphasizing Solid Materials and Systems, Wiley, New York, 1987.
[33] E.P. Murray, S.A. Barnett, Solid State Ionics 143 (2001) 265–273.
[34] S.W. Baek, J.H. Kim, J. Bae, Solid State Ionics 179 (2008) 1570–1574.
[35] B.C.H. Steele, Solid State Ionics 86–88 (1996) 1223–1234.
[36] E.P. Murray, M.J. Sever, S.A. Barnett, Solid State Ionics 148 (2002) 27–34.
[37] H. Lv, Y.J. Wu, B. Huang, B.Y. Zhao, K.A. Hu, Solid State Ionics 177 (2006) 901–906.
[38] S.G. Huang, C.Q. Peng, Z. Zong, J. Power Sources 176 (2008) 102–106.